PHYSICAL REVIEW B **89**, 174303 (2014)

Dynamics of coherent acoustic phonons in thin films of $CoSb_3$ and partially filled $Yb_xCo_4Sb_{12}$ skutterudites

Chuan He,[1,*] Marcus Daniel,[2] Martin Grossmann,[1] Oliver Ristow,[1] Delia Brick,[1] Martin Schubert,[1] Manfred Albrecht,[2,†] and Thomas Dekorsy[1]

[1]*Department of Physics, University of Konstanz, 78457 Konstanz, Germany*

[2]*Institute of Physics, Chemnitz University of Technology, 09107 Chemnitz, Germany*

(Received 27 February 2014; published 20 May 2014)

Skutterudites are considered as interesting material for thermoelectric applications. Filling foreign atoms into the cagelike structure of a $CoSb_3$ skutterudite is beneficial to its thermoelectric properties by increasing phonon scattering while maintaining the electrical conductivity. In this paper we demonstrate the generation and detection of coherent acoustic phonons in thin films of $CoSb_3$ and partially filled $Yb_xCo_4Sb_{12}$ skutterudites using femtosecond pump-probe spectroscopy. By using a pulse-echo method, the longitudinal sound velocity of amorphous and polycrystalline $CoSb_3$ thin films is obtained. For partially filled $Yb_xCo_4Sb_{12}$ thin films, an obvious decrease of the longitudinal sound velocity is observed at high filling fraction. Concomitantly, the high frequency acoustic phonon modes are strongly damped as the Yb filling fraction increases, which gives direct evidence for acoustic phonon scattering processes. It is shown that the reduction of lattice thermal conductivity after Yb filling is mainly achieved by the strong scattering of acoustic phonons.

DOI: 10.1103/PhysRevB.89.174303 PACS number(s): 63.20.−e, 43.35.Ud, 62.80.+f, 68.60.Bs

I. INTRODUCTION

Skutterudites have attracted much attention as new thermoelectric material due to their capability of achieving low lattice thermal conductivity while maintaining good electronic properties [1–6]. The unit cell of binary skutterudites MX_3 (M = Co,Fe,Rh,Ir; X = Sb,As,P) consists of eight cages formed by M atoms and six near-square X_4 rings residing inside each of the cages, as is shown in Fig. 1(a). The lattice thermal conductivity κ_l of skutterudites can be greatly suppressed through structural engineering, such as filling foreign atoms in the remaining voids or distorting the near-square X_4 rings by substitution [4,6,7]. Partial void -filling is of particular interest, hence the vibrational properties of partially filled $R_xM_4X_{12}$ (R = Mn,La,Ce,Yb,Nd,Tl) skutterudites have been intensively investigated in order to elucidate the effect of foreign atoms on heat-carrying phonons [6,8–12]. The foreign atoms are loosely bound in the atomic cage, making filled skutterudites a model system for heat transport and phonon scattering [13]. Acoustic phonons, which involve the collective motion of the atoms, are believed to be strongly scattered in the presence of foreign atoms and thus impede the heat transport [6,11]. The foreign atoms, which exhibit localized vibrations in the oversized cages, can be described as Einstein oscillators [6,8,9,13], or they are considered to be coupled to the host lattice [10,11]. For higher energy optical phonons, the vibrational modes are Raman active and correspond to the vibrations of X_4 rings [14]. The broadening and shift of these modes are a consequence of the filling. This suggests an interaction between the foreign atoms and the optical phonons, which leads to reduced thermal conductivity [14,15].

In this paper, we demonstrate the generation and detection of coherent acoustic phonons in thin films of $CoSb_3$ and partially filled $Yb_xCo_4Sb_{12}$ skutterudites. The $CoSb_3$ thin films of various film thicknesses and the $Yb_xCo_4Sb_{12}$ thin films of different filling fraction x were deposited on SiO_2/Si(100) substrates and investigated using femtosecond pump-probe spectroscopy. The analysis of the acoustic dynamics of these thin films allows us to obtain deeper knowledge of the effect of the Yb atoms on heat transport in partially filled skutterudites.

II. EXPERIMENTAL DETAILS

$CoSb_3$ thin films were deposited at room temperature on SiO_2(100 nm)/Si(100) substrates in an ultrahigh vacuum (UHV) chamber with a base pressure of 1×10^{-10} mbar. Sb was evaporated by an effusion cell, while Co in parallel by an electron beam evaporator. The rotation of the sample holder during the deposition ensured a homogenous composition. The composition and thickness of the as-deposited $CoSb_3$ films were measured by Rutherford backscattering spectrometry (RBS). The $CoSb_3$ composition could be confirmed and the corresponding film thicknesses were determined to be 8 ± 1 nm, 14 ± 1 nm, 27 ± 1 nm, 81 ± 1 nm, 139 ± 1 nm, 153 ± 1 nm, and 224 ± 1 nm. After a short exposure to air, a post-annealing treatment was followed at 500 °C for 1 hour in the UHV chamber. The thickness and the Sb content of the $CoSb_3$ thin films were slightly decreased after the post-annealing process. X-ray diffraction (XRD) results indicated that the as-deposited films were amorphous while the annealed films exhibited the polycrystalline skutterudite phase of $CoSb_3$ [16]. The $CoSb_3$ samples have a layer structure of $CoSb_3/SiO_2/Si(100)$. For brevity, the $CoSb_3/SiO_2$ interface and SiO_2/Si(100) interface will be referred to as 1st interface and 2nd interface, respectively. The crystal and sample structure of $CoSb_3$ skutterudite are illustrated in Figs. 1(a) and 1(b), respectively.

Partially filled $Yb_xCo_4Sb_{12}$ thin films were fabricated on SiO_2/Si(100) substrates by thermal evaporation in UHV at room temperature and post annealed for 1 hour at 300 °C and

*chuan.he@uni-konstanz.de

†Present address: Institute of Physics, University of Augsburg, Universitätsstr. 1, 86159 Augsburg, Germany.

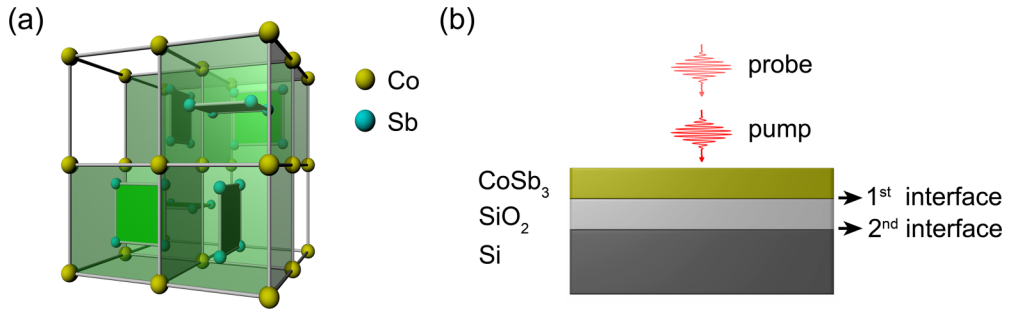

FIG. 1. (Color online) The crystal and sample structure of $CoSb_3$ skutterudite. (a) The cubic unit cell of $CoSb_3$ skutterudite. The Co (yellow) atoms form eight small cages and six of them are occupied by the planar square rings of four Sb (cyan) atoms. The remaining two empty cages can be filled by foreign atoms. (b) Graphical representation of the $CoSb_3$ sample with a layer structure of $CoSb_3/SiO_2$(100nm)/Si(100), which was investigated by femtosecond pump-probe spectroscopy.

500 °C to form the polycrystalline skutterudite phase of $CoSb_3$. Yb was evaporated by an effusion cell. To vary the Yb content x of the films, the Yb flux was adjusted while the Co and Sb flux remained constant during the fabrication process. The rare earth element Yb is chosen because it has been proven to be one of the most effective filling atoms for reducing the thermal conductivity of $CoSb_3$ [4,6]. The formation of the skutterudite phase was confirmed by XRD measurements and the filling fraction x of the $Yb_xCo_4Sb_{12}$ thin films was extracted by Rietveld refinement. For $Yb_xCo_4Sb_{12}$ thin films annealed at 300 °C, filling fractions of $x = 0, 0.08, 0.27$, and 0.68 were obtained, while for $Yb_xCo_4Sb_{12}$ thin films annealed at 500 °C, filling fractions of $x = 0, 0.05, 0.12$, and 0.57 were achieved. Details will be presented in a forthcoming publication. Composition and thickness of the $Yb_xCo_4Sb_{12}$ thin films were determined by RBS, and the effective charge carrier density was characterized by Hall measurements. Their structural and electrical properties are summarized in Table I. Hall measurements also revealed that the electrical conduction of the $CoSb_3$ thin films changes from p to n type after the Yb filling.

Coherent acoustic phonons are generated and detected in thin films of $CoSb_3$ and partially filled $Yb_xCo_4Sb_{12}$ skutterudites using high-speed asynchronous optical sampling (ASOPS) [17]. ASOPS is a femtosecond pump-probe technique that uses two mode-locked Ti:sapphire femtosecond lasers operating at a repetition rate of ~800 MHz. A stabilized frequency offset of 5 kHz in the repetition rate between pump and probe lasers enables the ASOPS system to scan the ultrafast dynamic processes in a measurement window of ~1.25 ns. The nominal pulse durations of pump and probe are ~50 fs and the wavelengths of pump and probe are set to 790 nm and 820 nm, respectively. All measurements are performed at room temperature in a collinear reflection geometry and the laser beams are focused on the samples with a spatial FWHM of the spots below ~2 μm. Since $CoSb_3$ is a narrow band-gap semiconductor [18], the intense ultrashort pump pulse absorbed will generate a large amount of nonequilibrium carriers. The fast relaxation of these carriers sets up an isotropic stress that launches a coherent longitudinal acoustic phonon pulse propagating away from the surface at the speed of sound [19,20]. As the acoustic pulse propagates it alters the local optical constants and the relative reflectivity change $\Delta R/R$ is detected by the time delayed probe pulses through acousto-optic interaction within the absorption depth.

III. RESULTS AND DISCUSSION

The ASOPS system allows the direct observation of carrier and phonon dynamics in $CoSb_3$ and $Yb_xCo_4Sb_{12}$ thin films in the time domain. Figures 2(a) and 2(c) illustrate the relative transient reflectivity changes of as-deposited and annealed $CoSb_3$ samples, respectively. In the first picoseconds, a drastic change in $\Delta R/R$ is observed in the samples. This rapid change is due to the nonequilibrium carriers generated in the samples after the absorption of the pump pulse. Subsequently the carriers transfer their excess energy to the lattice through electron-phonon scattering processes. The pump-excited acoustic pulses that propagate into the samples modulate the refractive index through photoelastic

TABLE I. The structural and electrical properties of $Yb_xCo_4Sb_{12}$ thin films.

Annealing temperature	Thickness (nm)	Composition	Yb filling fraction x	Effective carrier density (cm^{-3})	Longitudinal sound velocity (m/s)
300 °C	34 ± 1	$CoSb_{3.2}$	0	1.5×10^{20}	$(3.8 \pm 0.2) \times 10^3$
	45 ± 2	$Yb_{0.08}(CoSb_{3.4})_4$	0.08	1.7×10^{22}	$(4.2 \pm 0.3) \times 10^3$
	45 ± 2	$Yb_{0.23}(CoSb_{3.5})_4$	0.27	1.2×10^{22}	$(4.2 \pm 0.3) \times 10^3$
	49 ± 2	$Yb_{1.15}(CoSb_{3.2})_4$	0.68	3.9×10^{22}	$(3.8 \pm 0.3) \times 10^3$
500 °C	33 ± 1	$CoSb_{3.2}$	0	3.5×10^{19}	$(4.0 \pm 0.2) \times 10^3$
	42 ± 2	$Yb_{0.08}(CoSb_{3.2})_4$	0.05	1.8×10^{20}	$(4.3 \pm 0.3) \times 10^3$
	44 ± 2	$Yb_{0.29}(CoSb_{3.4})_4$	0.12	5.3×10^{20}	$(4.4 \pm 0.3) \times 10^3$
	49 ± 2	$Yb_{1.15}(CoSb_{3.2})_4$	0.57	9.3×10^{21}	$(4.1 \pm 0.3) \times 10^3$

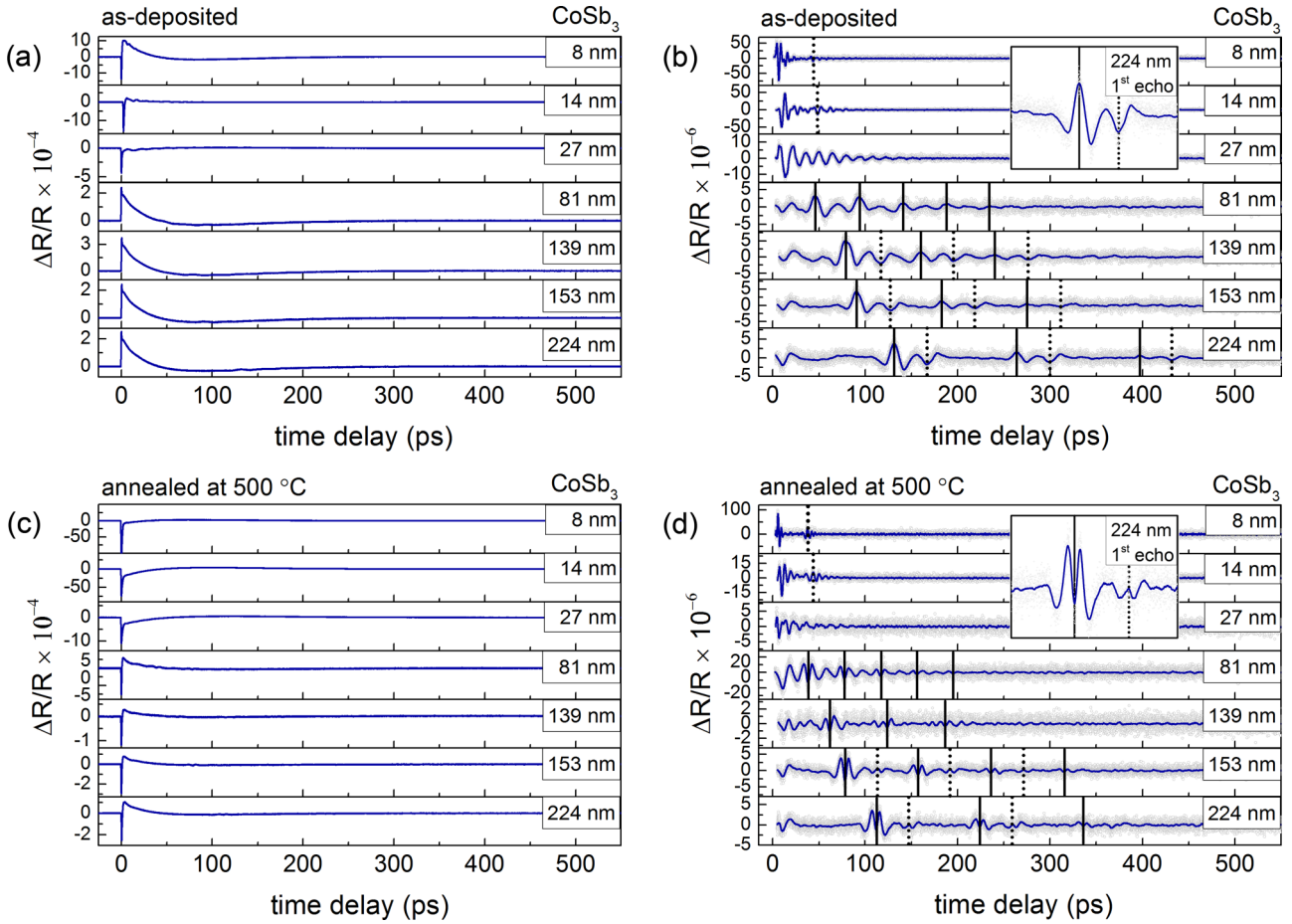

FIG. 2. (Color online) Transient reflectivity changes and the extracted reflectivity signals of $CoSb_3$ samples: (a) and (b) as-deposited; (c) and (d) annealed at 500°C. The extracted signals of as-deposited and annealed $CoSb_3$ samples change from damped oscillation to equally spaced echoes as the thickness of the $CoSb_3$ film increases. The damped oscillations arise from the interference of the probe light reflected at the surface and the acoustic pulse bounced inside the $CoSb_3$ films, while the equally spaced echoes result from the multiple reflections of acoustic pulses between the surface and the 1st interface. The insets in (b) and (d) are the respective close-up views of the 1st echo of the 224 nm samples. The solid and dotted lines indicate acoustic reflections from the 1st interface and the 2nd interface, respectively.

coupling. This leads to different signals, such as oscillations or echoes, that superimposed on the slowly decaying electronic background in $\Delta R/R$. The lattice contribution of as-deposited and annealed samples are shown in Figs. 2(b) and 2(d), respectively, after subtracting the electronic background. It can be seen that the reflectivity signals of as-deposited and annealed samples change gradually from damped oscillations to equally spaced echoes as the thickness of the $CoSb_3$ film increases.

Equally spaced echoes are clearly observed in the thicker $CoSb_3$ films with thickness of 81 nm, 139 nm, 153 nm, and 224 nm, where the film thicknesses are sufficiently large for the detection of separate echoes. In this case, the film thicknesses are larger than the absorption depth of the probe light and the acoustic pulses can only be detected each time they arrive at the surface. So the equally spaced echoes in each sample, which are indicated by the solid lines in Figs. 2(b) and 2(d), result from multiple reflections of the acoustic pulse between the free surface and the 1st interface of the corresponding $CoSb_3$ film. The spacing between the successive echoes gives the round-trip time τ_1 of the acoustic pulse traveling in the $CoSb_3$ film. Thus the longitudinal sound velocity can be obtained by $v_{CoSb_3} = 2d/\tau_1$, where d is the film thickness. For as-deposited and annealed $CoSb_3$ films the longitudinal sound velocities are calculated to be $(3.39 \pm 0.01) \times 10^3$ m/s and $(4.05 \pm 0.11) \times 10^3$ m/s, respectively. The increase of the sound velocity for the $CoSb_3$ films is attributed to the fact that the as-deposited $CoSb_3$ films crystallize during the annealing process and the skutterudite phase is formed. It is noteworthy that using the pulse-echo method the accuracy of the longitudinal sound velocity for the $CoSb_3$ films is better than that of the $Yb_xCo_4Sb_{12}$ films with $x = 0$ (see Table I), which is obtained later using a different method.

It is also noticeable that the amplitudes of these echoes decrease as the acoustic pulses travel inside the films. This reflects the attenuation of propagating acoustic pulse and the fact that part of the pulse is transmitted across the interfaces [19]. When the acoustic pulse arrives at the 1st interface, part of this pulse is reflected at this interface, while the rest of the pulse will transmit into the SiO_2 layer and then be partially reflected at the 2nd interface. The fraction of an acoustic pulse reflected at the interface between material a and material b is determined by the reflection coefficient $r = (Z_b - Z_a)/(Z_b + Z_a)$, where Z is the acoustic impedance of a

TABLE II. Round-trip time of acoustic pulses traveling through the $CoSb_3$ films and SiO_2 layers.

	Round-trip time τ_{rt} (ps)	
Sample	Calculated	Experiment
as-deposited 8 nm	38.2 ± 0.9	43.6 ± 0.2
as-deposited 14 nm	41.8 ± 0.9	48.7 ± 0.2
annealed 8 nm	37.5 ± 0.9	37.7 ± 0.2
annealed 14 nm	40.4 ± 1	42.9 ± 0.2

material that equals the product of density ρ and longitudinal sound velocity v_l [21]. Using the sound velocity obtained, the reflection coefficient r_1 at the 1st interface for as-deposited and annealed samples is -0.33 and -0.41, respectively, assuming the theoretical density of 7.621 g/cm^3 of single crystal $CoSb_3$ for both as-deposited and annealed films [22]. The density and longitudinal sound velocity of SiO_2 are $\rho_{SiO_2} = 2.20$ g/cm^3 and $v_{SiO_2} = 5970$ m/s, respectively [23]. The negative reflection coefficient means that the $CoSb_3$ films have a larger acoustic impedance than the SiO_2 layer and hence the acoustic pulse undergoes a phase change of π upon reflection from the 1st interface. Since the acoustic pulse will also be reflected with a phase change of π at the surface, the equally spaced echoes exhibit a similar shape upon returning again to the surface. As stated before, echoes reflected at the 2nd interface will come τ_2 later than the ones from the 1st interface, where τ_2 is the round-trip time of acoustic pulse traveling in the SiO_2 layer. Therefore wide separations between the equally spaced echoes are required for observing the echoes reflected at the 2nd interface. These echoes are indicated by the dotted lines in Figs. 2(b) and 2(d). Using the sound velocity of 5970 m/s for SiO_2 [23], τ_2 is calculated to be 33.5 ps, which is close to the experimental value of 36.1 ps. At the 2nd interface, no phase change occurs since the reflection coefficient r_2 equals 0.20, where $\rho_{SiO_2} = 2.20$ g/cm^3, $v_{SiO_2} = 5970$ m/s and $\rho_{Si} = 2.33$ g/cm^3, $v_{Si} = 8430$ m/s [23]. So the echoes reflected from the 2nd interface have inverted shapes compared with the ones from the 1st interface. The insets in Figs. 2(b) and 2(d) are the close-up views of the 1st echo of as-deposited and annealed 224 nm film samples, respectively, where the echoes reflected from both interfaces are clearly separated in time.

For the thinner $CoSb_3$ films with thickness of 8 nm, 14 nm, and 27 nm, the initial fast damped oscillations arise from the interference of the probe light reflected at the surface and acoustic pulses bounced between the surface and the 1st interface of these films [19]. In addition, echo signals, which are also labeled by the dotted lines in Figs. 2(b) and 2(d), are observed in the time domain for the 8 nm and the 14 nm film samples. These echoes are attributed to the acoustic pulses

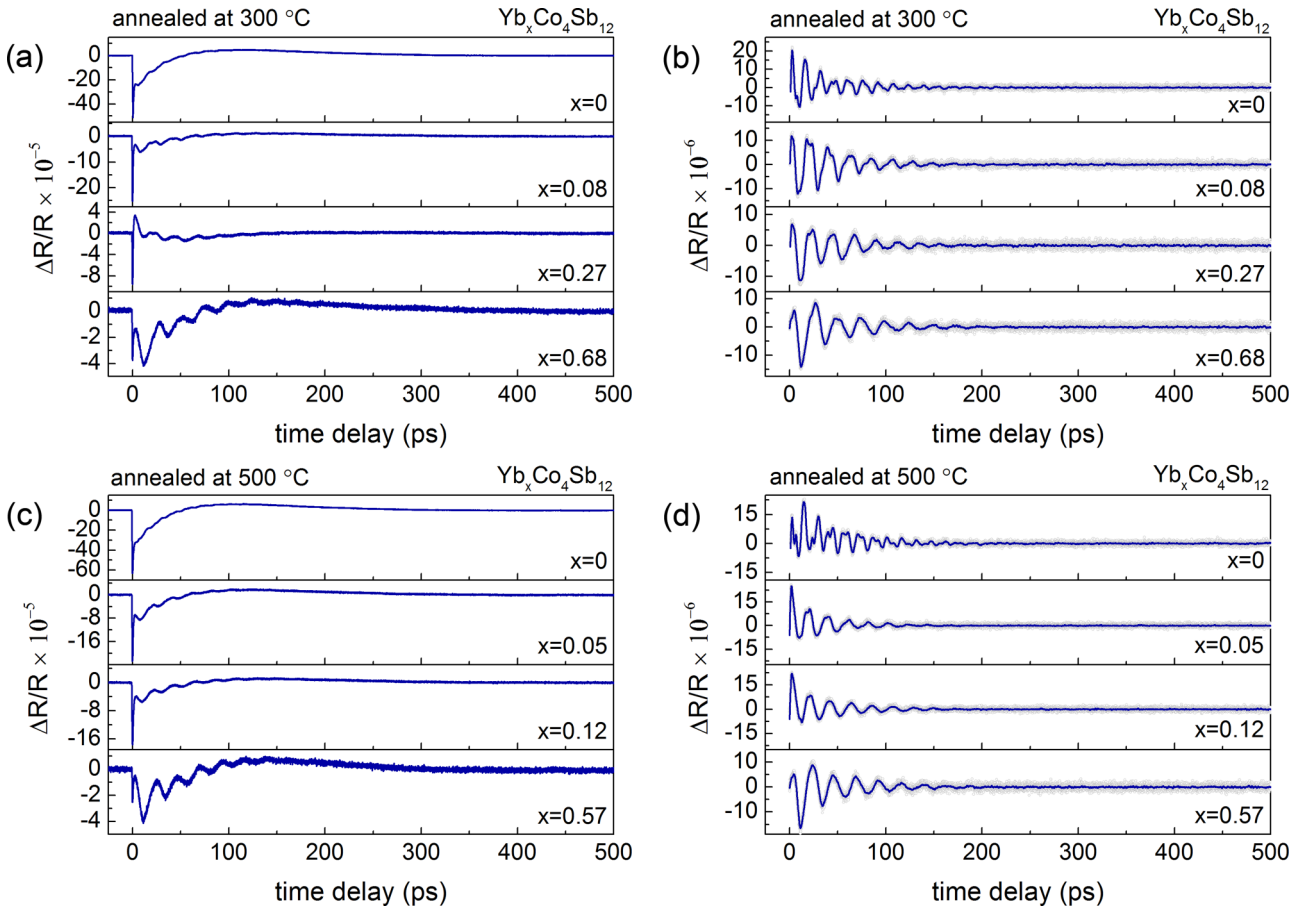

FIG. 3. (Color online) Transient reflectivity changes and the extracted reflectivity signals of $Yb_xCo_4Sb_{12}$ samples: (a) and (b) annealed at 300 °C; (c) and (d) annealed at 500 °C. The film thicknesses, which vary from 33 nm to 49 nm, are listed in Table I. An obvious decrease of the magnitude of the electronic contribution to $\Delta R/R$ is observed as the filling fraction x increases in both (a) and (c), which is probably due to the increase of carrier concentration as a consequence of filling.

reflected at the 2nd interface and the arrival time of the echoes corresponds to the round-trip time τ_{rt} ($\tau_{rt} = \tau_1 + \tau_2$) of acoustic pulses traveling through both the $CoSb_3$ films and the SiO_2 layers. The calculated and experimental values of τ_{rt} for as-deposited and annealed samples with thicknesses of 8 nm and 14 nm are listed in Table II. Since the echoes are reflected from the 2nd interface, the shapes of echoes in the thinner films are also inverted compared with the ones reflected at the 1st interface of corresponding thicker samples.

In order to study the effect of foreign atoms on the heat transport in $CoSb_3$ skutterudite, $Yb_xCo_4Sb_{12}$ thin films with different filling fraction x were also investigated. The transient reflectivity changes of the $Yb_xCo_4Sb_{12}$ film samples annealed at 300 °C and 500 °C are depicted in Figs. 3(a) and 3(c), respectively. As can be seen, there is an obvious decrease of the magnitude of the electronic contribution to $\Delta R/R$ as the filling fraction x increases. This rapid decrease is probably due to the fact that the carrier concentration typically increases by several orders of magnitude as a consequence of filling, as listed in Table I. Hence the optically excited carrier density becomes much smaller than the background carrier concentration. The superimposed oscillations are extracted and shown in Figs. 3(b) and 3(d), where damped oscillations are seen for all the samples with comparable amplitude. Figure 4 shows the fast Fourier transform (FFT) of the extracted oscillations, in which nearly equidistant peaks are seen for different x. The nearly equidistant peaks in the phonon spectra are due to the confinement of the acoustical vibrations in the planar phonon cavity formed by the surface of the $Yb_xCo_4Sb_{12}$ film and its interface with the SiO_2 layer [24]. The negative acoustic mismatch between the $Yb_xCo_4Sb_{12}$ film and the SiO_2 layer gives rise to acoustic resonances when the wave vectors satisfies the condition: $k_m = m\pi/d$, where d is the film thickness and m is the mode number [23]. As is shown in Fig. 4, when $x = 0$, a series of phonon modes up to the 5th harmonic is observed; after the Yb filling, the high frequency phonon modes are strongly suppressed. The suppression of the phonon modes gives evidence of the scattering of acoustic phonons in the presence of Yb atoms.

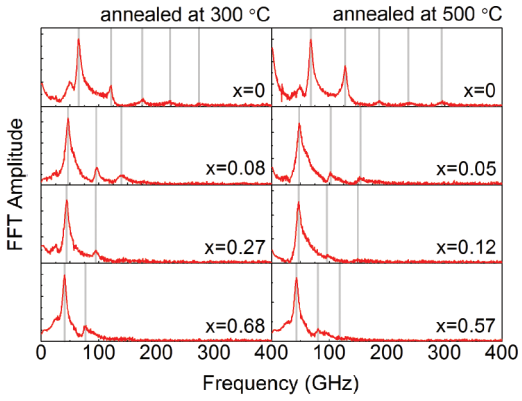

FIG. 4. (Color online) Fast Fourier transform of the $Yb_xCo_4Sb_{12}$ transient shown in Fig. 3. The phonon spectra are discretized due to the confinement of the acoustical vibrations in the $Yb_xCo_4Sb_{12}$ films. As the filling fraction increases, the high-frequency phonons are strongly suppressed. The suppression of phonon peaks gives evidence of the scattering of acoustic phonons in the presence of the Yb atoms.

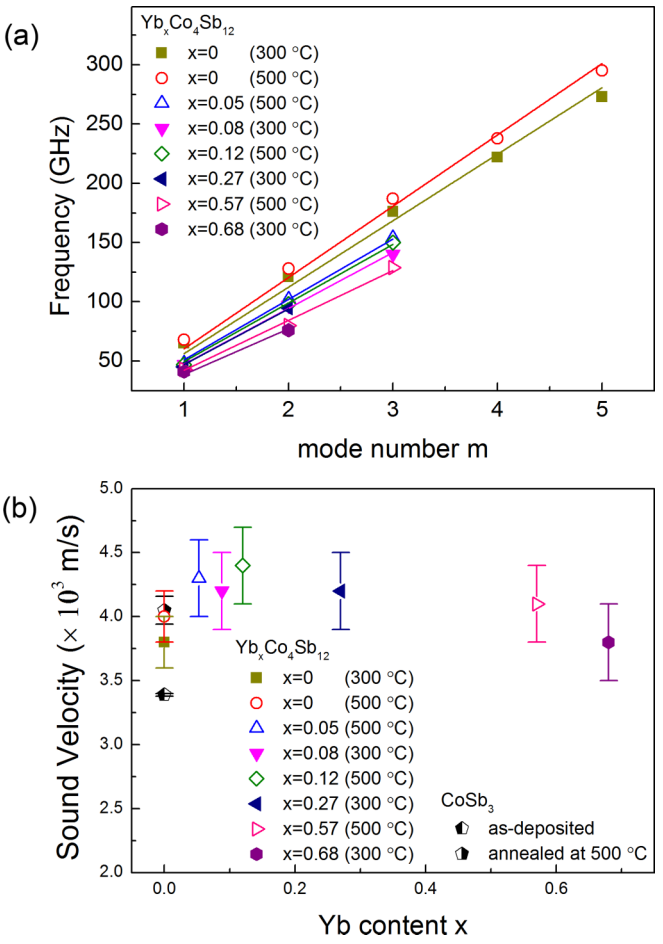

FIG. 5. (Color online) (a) The frequency of the peaks in Fig. 4 is plotted over mode number m. The linear fits for $Yb_xCo_4Sb_{12}$ samples are also shown. (b) Plot of calculated sound velocity over Yb content x. The sound velocities of $CoSb_3$ films are depicted for comparison. A significant drop of the sound velocity in $Yb_xCo_4Sb_{12}$ samples is observed at high filling fraction. At $x = 0.68$ the sound velocity is comparable to that of polycrystalline $CoSb_3$ films. Filled and open symbols represent $Yb_xCo_4Sb_{12}$ samples annealed at 300 °C and 500 °C, respectively.

In the Debye model with $\omega = v_l k$, the relationship between the discrete frequency f_m and the film thickness d is $f_m = mv_l/2d$. The frequency of the peaks f_m is plotted over the mode number m in Fig. 5(a). Provided the thicknesses d in Table I, the longitudinal sound velocities v_l of the $Yb_xCo_4Sb_{12}$ films are obtained (see Table I) and plotted in Fig. 5(b), in which the value of v_l of as-deposited and annealed $CoSb_3$ films are also given for comparison. At $x = 0$, v_l for the annealed samples increases as the annealing temperature rises. This increase is due to the improved crystallinity with higher annealing temperatures. The difference of v_l between the $CoSb_3$ film and the $Yb_xCo_4Sb_{12}$ film with $x = 0$, which were both annealed at 500 °C, may arise from the uncertainty of the measured film thickness. For partially filled $Yb_xCo_4Sb_{12}$ skutterudites, in the low filling fraction region ($0 < x < 0.3$), v_l are increased as a consequence of filling. As the filling fraction x increases ($x > 0.3$), an obvious decrease of v_l is observed, and at the highest filling fraction of $x = 0.68$, v_l is

reduced to a value comparable to that of polycrystalline $CoSb_3$. In contrast to the influence of filling on the acoustic phonon modes, where noticeable effect occurs at a filling fraction lower than 0.3, the significant drop of v_l is only observed at high filling fraction. Since the structure of skutterudite is well maintained after filling, the decrease of v_l is primarily ascribed to the presence of Yb atoms.

The lattice thermal conductivity κ_l can be estimated using the kinetic theory of gases [12,25]:

$$\kappa_l = \tfrac{1}{3} C_V v_m l = \tfrac{1}{3} C_V v_m^2 \tau, \quad (1)$$

where C_V is the heat capacity per unit volume, v_m the mean sound velocity of the phonons, l the mean free path of the phonons, τ the phonon relaxation time. The mean sound velocity v_m is obtained from $3v_m^{-3} = v_l^{-3} + 2v_t^{-3}$, where v_t and v_l are the transverse and longitudinal sound velocity, respectively. According to Eq. (1), the low κ_l can be achieved by decreasing v_m, or shortening τ through phonon scattering processes. It has been experimentally confirmed that the κ_l of $CoSb_3$ decreases upon Yb filling [4,26]. In the low filling fraction region, where an increase of v_l is observed, the reduction of κ_l is mainly achieved by the strong scattering of the high frequency acoustic phonons, which leads to a reduction of τ. At high filling fraction of $x = 0.57$ and 0.68, the significant drop of v_l, together with the strong scattering of acoustic phonons, could lead to a further reduction of κ_l. As listed in Table I, even at $x = 0.68$, v_l is still comparable to that of polycrystalline $CoSb_3$, so despite the drop of v_l at high filling fraction, the dominant mechanism in the reduction of κ_l after filling is the stronger scattering of acoustic phonons, which shorten the phonon relaxation time τ.

IV. CONCLUSION

In conclusion, thin films of $CoSb_3$ and partially filled $Yb_xCo_4Sb_{12}$ skutterudites were fabricated on SiO_2(100 nm)/Si (100) substrates in an UHV chamber and investigated by a femtosecond pump-probe spectroscopy. Using a pulse-echo method the longitudinal sound velocities of amorphous and polycrystalline $CoSb_3$ thin films are determined to be $(3.39 \pm 0.01) \times 10^3$ m/s and $(4.05 \pm 0.11) \times 10^3$ m/s, respectively, while the confinement of the acoustical vibrations are observed in the partially filled $Yb_xCo_4Sb_{12}$ thin films. The suppression of high frequency acoustic phonons as a consequence of filling provides evidence for the enhanced scattering of acoustic phonons in the presence of Yb atoms. As the filling fraction x increases, an obvious decrease of the sound velocity is observed, and at the highest filling fraction of $x = 0.68$ the sound velocity is reduced to a value comparable to that of polycrystalline $CoSb_3$. Our results clearly demonstrate that the scattering of acoustic phonons dominates the reduction of lattice thermal conductivity in the partially filled $Yb_xCo_4Sb_{12}$ skutterudites.

ACKNOWLEDGMENTS

This work was supported by the German Research Foundation (DFG) through the SFB 767 and SPP 1386 (Germany) and by the Ministry of Science, Research and Arts of Baden-Württemberg (Germany). We acknowledge the helpful discussions with V. Gusev at Université du Maine (France). We also would like to thank the Helmholtz-Zentrum Dresden-Rossendorf e.V. (Germany) for RBS measurements and especially R. Willhelm for his scientific support. The authors gratefully acknowledge the financial support from the China Scholarship Council (CSC).

[1] G. S. Nolas, G. A. Slack, D. T. Morelli, T. M. Tritt, and A. C. Ehrlich, J. Appl. Phys. **79**, 4002 (1996).
[2] G. S. Nolas, J. L. Cohn, and G. A. Slack, Phys. Rev. B **58**, 164 (1998).
[3] G. S. Nolas, D. T. Morelli, and T. M. Tritt, Annu. Rev. Mater. Sci. **29**, 89 (1999).
[4] G. S. Nolas, M. Kaeser, R. T. Littleton IV, and T. M. Tritt, Appl. Phys. Lett. **77**, 1855 (2000).
[5] B. C. Sales, D. Mandrus, B. C. Chakoumakos, V. Keppens, and J. R. Thompson, Phys. Rev. B **56**, 15081 (1997).
[6] J.-L. Mi, M. Christensen, E. Nishibori, and B. B. Iversen, Phys. Rev. B **84**, 064114 (2011).
[7] H. Chi, H. Kim, J. C. Thomas, X. Su, S. Stackhouse, M. Kaviany, A. Van der Ven, X. Tang, and C. Uher, Phys. Rev. B **86**, 195209 (2012).
[8] R. P. Hermann, R. Jin, W. Schweika, F. Grandjean, D. Mandrus, B. C. Sales, and G. J. Long, Phys. Rev. Lett. **90**, 135505 (2003).
[9] V. Keppens, D. Mandrus, B. C. Sales, B. C. Chakoumakos, P. Dai, R. Coldea, M. B. Maple, D. A. Gajewski, E. J. Freeman, and S. Bennington, Nature (London) **395**, 876 (1998).
[10] M. M. Koza, M. R. Johnson, R. Viennois, H. Mutka, L. Girard, and D. Ravot, Nat. Mater. **7**, 805 (2008).
[11] Y. Wang, X. Xu, and J. Yang, Phys. Rev. Lett. **102**, 175508 (2009).
[12] M. Christensen, A. B. Abrahamsen, N. B. Christensen, F. Juranyi, N. H. Andersen, K. Lefmann, J. Andreasson, C. R. H. Bahl, and B. B. Iversen, Nat. Mater. **7**, 811 (2008).
[13] R. P. Hermann, F. Grandjean, and G. J. Long, Am. J. Phys **73**, 110 (2005).
[14] G. S. Nolas and C. A. Kendziora, Phys. Rev. B **59**, 6189 (1999).
[15] G. S. Nolas, G. A. Slack, T. Caillat, and G. P. Meisner, J. Appl. Phys. **79**, 2622 (1996).
[16] M. Daniel, M. Friedemann, N. Jöhrmann, A. Liebig, J. Donges, M. Hietschold, G. Beddies, and M. Albrecht, Phys. Status Solidi A **210**, 140 (2013).
[17] R. Gebs, G. Klatt, C. Janke, T. Dekorsy, and A. Bartels, Opt. Express **18**, 5974 (2010).
[18] D. J. Singh and W. E. Pickett, Phys. Rev. B **50**, 11235 (1994).
[19] C. Thomsen, H. T. Grahn, H. J. Maris, and J. Tauc, Phys. Rev. B **34**, 4129 (1986).

[20] O. B. Wright, B. Perrin, O. Matsuda, and V. E. Gusev, Phys. Rev. B **64**, 081202 (2001).
[21] H. N. Lin, R. J. Stoner, H. J. Maris, and J. Tauc, J. Appl. Phys. **69**, 3816 (1991).
[22] T. Caillat, A. Borshchevsky, and J. P. Fleurial, J. Appl. Phys. **80**, 4442 (1996).
[23] J. Groenen, F. Poinsotte, A. Zwick, C. M. Sotomayor Torres, M. Prunnila, and J. Ahopelto, Phys. Rev. B **77**, 045420 (2008).
[24] F. Hudert, A. Bruchhausen, D. Issenmann, O. Schecker, R. Waitz, A. Erbe, E. Scheer, T. Dekorsy, A. Mlayah, and J.-R. Huntzinger, Phys. Rev. B **79**, 201307(R) (2009).
[25] E. S. Toberer, A. Zevalkink, and G. J. Snyder, J. Mater. Chem. **21**, 15843 (2011).
[26] J. Yang, Q. Hao, H. Wang, Y. C. Lan, Q. Y. He, A. Minnich, D. Z. Wang, J. A. Harriman, V. M. Varki, M. S. Dresselhaus, G. Chen, and Z. F. Ren, Phys. Rev. B **80**, 115329 (2009).